Molecular Neurobiology (2019) 56:3244–3259
https://doi.org/10.1007/s12035-018-1301-8

Targeting Axon Integrity to Prevent Chemotherapy-Induced Peripheral Neuropathy

Virendra Bhagawan Chine[1] · Ngan Pan Bennett Au[1] · Gajendra Kumar[1] · Chi Him Eddie Ma[1,2]

Received: 15 May 2018 / Accepted: 2 August 2018 / Published online: 16 August 2018

Abstract

Chemotherapy-induced peripheral neuropathy (CIPN) is an irreversible off-target adverse effect of many chemotherapeutic agents such as paclitaxel, yet its mechanism is poorly understood and no preventative measure is available. CIPN is characterized by peripheral nerve damages resulting in permanent sensory function deficits. Our recent unbiased genome-wide analysis revealed that heat shock protein (Hsp) 27 is part of a transcriptional network induced by axonal injury and highly enriched for genes involved in adaptive neuronal responses, particularly axonal regeneration. To examine if Hsp27 could prevent the occurrence of CIPN, we first demonstrated that paclitaxel-induced allodynia was associated directly with axonal degeneration in sensory neurons in a mouse model of CIPN. We therefore hypothesize that by preventing axonal degeneration could prevent the development of CIPN. We drove expression of human Hsp27 (hHsp27) specifically in neurons. Development of mechanical and thermal allodynia was prevented completely in paclitaxel-treated hHsp27 transgenic mice. Strikingly, hHsp27 protected against paclitaxel-induced neurotoxicity in vivo including degeneration of afferent nerve fibers, demyelination, mitochondrial swelling, apoptosis, and restored sensory nerve action potential. Finally, we delineated signaling cascades that link CIPN development to caspase 3 and RhoA/cofilin activation in sensory neurons and peripheral nerves. hHsp27 exerted anti-apoptotic effect and maintained axon integrity by restoring caspase 3 and RhoA expression to basal levels. Taken together, our data suggest that by preventing axonal degeneration might prove beneficial as anti-CIPN drugs, which represents an emerging research area for therapeutic development.

Keywords Chemotherapy-induced peripheral neuropathy · Heat shock protein 27 · Paclitaxel · Axonal degeneration · Apoptosis

Introduction

Chemotherapy refers to the treatment of cancer with antineoplastic drugs (preventing growth and proliferation of malignant cells) which target mainly proliferating cells (i.e., cancer cells); however, for some unknown reasons, chemotherapy drugs also damage healthy neuronal cells [1, 2]. The absence of an effective blood-nerve barrier in sensory neurons and nerves of the peripheral nervous system are at increased risk, as compared to the central nervous system which is well protected by blood-brain barrier. An estimated of 40–50% of cancer patients undergo chemotherapy often experience sensory and motor symptoms such as numbness, tingling, weakness of distal muscle, and loss of motor control, a condition known as chemotherapy-induced peripheral neuropathy (CIPN) [3–6]. There is currently no prevention or effective treatment for CIPN, although it is one of the most common reasons that cancer patients discontinue their life-saving treatments.

Commonly used chemotherapy drugs associated with CIPN such as paclitaxel (Taxol®) are used for the treatment of solid carcinomas including ovarian, breast, and lung cancers [7, 8]. The anti-cancer action of paclitaxel is due to their binding to β-tubulin (major component of microtubule and axon) which disrupts mitotic spindle formation in actively dividing cells [7, 9, 10]. More than 50% of patients treated with paclitaxel describe a sensation of tingling, burning, and numbness in 24–72 h after administration [11]. Animal model

Electronic supplementary material The online version of this article (https://doi.org/10.1007/s12035-018-1301-8) contains supplementary material, which is available to authorized users.

✉ Chi Him Eddie Ma
eddiema@cityu.edu.hk

[1] Department of Biomedical Sciences, City University of Hong Kong, Tat Chee Avenue, Kowloon Tong, Hong Kong

[2] Centre for Biosystems, Neuroscience, and Nanotechnology, City University of Hong Kong, Tat Chee Avenue, Kowloon Tong, Hong Kong

of CIPN reproduces human condition which is widely used to study possible preventive interventions for peripheral neuropathy [12–17]. Intraperitoneal (i.p.) injection of paclitaxel induces loss of epidermal sensory fibers in hindpaw resulting in pain hypersensitivity in rodent [12, 17, 18] and axonal degeneration of peripheral nerves resulting in motor function impairments. Animal studies showed that circulating chemotherapy agents access injured nerves and adversely affect nerve repair [13, 14, 19, 20]. The mechanisms of CIPN remain unclear and controversial, but several studies show that neurotoxic chemotherapeutic agents cause irreversible injury to peripheral nerves by damaging microtubule, interfering with axonal transport, as well as causing neuronal cell death through their cytotoxic effects on DNA [2, 10]. Our recent study clearly demonstrated the direct effect of paclitaxel on inducing excessive microtubule polymerization in primary dorsal root ganglion (DRG) neurons [1]. If this is correct, an approach that stabilizes microtubule, accelerates axonal regeneration, and augments intrinsic growth pathways would prevent the range of abnormalities that develop during CIPN.

Our unbiased genome-wide analysis reveal that heat shock protein (Hsp) 27 is part of a transcriptional network induced by axonal injury and highly enriched for genes involved in adaptive neuronal responses, particularly axonal regeneration and survival [21]. Hsp27 is a chaperone protein and induced in many types of tissue when exposed to biological stress and acts to protect them from insults such as heat stress, oxidative stress, and ischemia [22–24]. Injury to peripheral axons and neurons produce profound changes in their cell bodies and actin cytoskeleton. Hsp27 is well-known for its interaction with actin and microtubule stabilization [25]. As an actin capping protein, Hsp27 binds to barbed ends of actin filaments and regulates actin polymerization [26–28]. Administration of anti-Hsp27 antibody to human eyes induced degradation of actin cytoskeleton in retinal cells in a dose-dependent manner. Anti-Hsp27 antibody binds to actin to induce depolymerization and proteolytic cleavage of actin, resulting in cytoskeleton breakdown [29]. More importantly, our earlier studies showed for the first time that chemotherapy drugs directly affect the regenerative capacity, cytoskeleton arrangement, and cell mechanical properties of primary sensory neurons [1]. Current study aims to realize clinical benefits of neurorestorative therapy targeting neuronal survival and axon integrity in a mouse model of CIPN. These findings form the basis of our hypothesis that forced expression of human Hsp27 (hHsp27) rendered CIPN with paclitaxel protects peripheral neurons and fibers from progressive degeneration. We first showed that primary DRG neurons purified from hHsp27 transgenic (Tg) mice were protected from paclitaxel-induced neurite outgrowth inhibition. We then extended the in vitro findings to in vivo functional recovery in hHsp27 Tg mice after paclitaxel injection as evaluated with a battery of animal behavioral, electrophysiological, and histological tests. hHsp27 forced expression specifically in neurons reverse paclitaxel-induced CIPN in mice via the anti-apoptotic (caspase 3) and axon integrity (RhoA/cofilin) signaling pathways.

Materials and Methods

Animals

Adult male hHsp27 Tg and LM mice (8–12 weeks old) were used for all experiments. We used Thy1.2 neuronal promoter to ensure postnatal expression of hHsp27 only in neurons [21] which do not affect normal development of nervous system and maintains expression at high levels throughout adulthood [30]. We backcrossed hHsp27 Tg mouse onto a C57BL/6 background to ensure that our data is comparable to the most widely used C57BL/6 mouse strain from other CIPN studies [15]. Mice were housed randomly in groups of 5–6 per cage and allowed food and water ad libitum. Light/dark cycle of 12:12 h was maintained and behavioral testing was conducted between 10 am and 6 pm. Animal experiments and euthanasia were performed in compliance with Institutional Animal Care and Use Committee guidelines and approved by the Animal Research Ethics Sub-Committee at City University of Hong Kong and Department of Health, HKSAR.

Primary Dissociated DRG Cultures

Primary dissociated DRG neurons were prepared from adult hHsp27 Tg or LM mice (8–12 weeks) as described [1, 21, 31]. In brief, DRGs were dissected out, digested with collagenase/dispase II (Roche Diagnostics), trypsinized, and mechanically dissociated using flame-polished Pasteur pipettes. A total of 2000 DRG neurons were plated onto poly-D-lysine and laminin (Sigma-Aldrich)-coated 8-well chamber slide (Millipore) and grown in Neurobasal (NB) medium supplemented with B27, 200 mM L-glutamine, penicillin/streptomycin, 50 ng/ml NGF (Gibco), 2 ng/ml GDNF, and 10 μM Ara-C (Sigma-Aldrich). After 1 h of plating, paclitaxel (Bristol-Myers Squibb) was applied to the cultures at a final concentration of 25 ng/ml, 50 ng/ml, 100 ng/ml, 1 μg/ml, or 10 μg/ml, and 0.1% Cremophor EL/ethanol (50:50) was used as vehicle control. The cultures were allowed to grow for 17 h and subjected to neurite outgrowth assay.

Neurite Outgrowth and Cell Survival Assay

After 17 h of incubation, DRG neurons were fixed with 4% paraformaldehyde (PFA) for 15 min, blocked with 0.5% bovine serum albumin/0.1% Triton X-100 (Sigma-Aldrich) for 1 h, and incubated with anti-βIII-tubulin (Sigma-Aldrich) overnight at 4 °C. The cultures were then washed with PBS

and incubated with secondary antibodies conjugated with Alexa Fluor 488 for neurite outgrowth and cell survival assay.

Neurite outgrowth assay was performed as described [1, 21]. Thirty non-overlapping images were taken at 10× magnifications using an epifluorescence microscope (Nikon Eclipse 90i) equipped with a motorized stage. Total neurite length of individual DRG neurons from each condition was determined using an automated WIS-NeuroMath software (Weizmann Institute of Science). Total neurite length was measured from at least 250 neurons in each experimental condition. βIII-tubulin-positive neurons with bright cell bodies and intact neurites were counted as healthy neurons. Data was obtained from three independent experiments repeated in duplicates.

Paclitaxel Administration

To examine the protective effects of hHsp27 on CIPN in vivo, hHsp27 Tg and LM mice were i.p. injected according to schedule described in details as follow: Paclitaxel (Taxol®) (Bristol-Myers-Squibb; 6 mg/ml) was dissolved in Cremophor EL/ethanol (50:50) and further diluted with saline to 1 mg/ml. Each mouse will receive four i.p. injections of paclitaxel (1 mg/kg) in total or saline on alternating successive days (days 0, 2, 4, and 6, $n = 11$ to 16 per genotype) [15, 32, 33].

Animal Behavioral Tests

Behavioral tests were performed in a quiet and temperature-controlled room. Behavioral scoring was done blinded to genotype and treatments. Last baseline behavioral measurements were obtained on day 0 before the first paclitaxel administration. von Frey filament was performed on days 0, 3, 6, 8, 12, 16, 20, 24, and 28. Acetone drop test was performed on days 0, 5, 7, 10, 15, 20, 25, and 30. Left and right hindpaw were tested since paclitaxel produced a bilateral neuropathy [12, 15]. We performed behavioral tests on left hindpaw first and waited for at least 1 h to test right paw of the same animal.

von Frey Filament Test

von Frey filament test was used to quantify mechanical allodynia [34, 35]. Adult mice were habituated in three separate sessions with handling reduced to a minimum and placed on an elevated wire mesh platform in boxes made of the same mesh material for 30 min sessions. On 3 days, spread over a 1-week period, baseline values were obtained for response to mechanical stimulation using von Frey monofilaments (Bioseb). The average of three values prior to injection was recorded as baseline. von Frey filaments in the range of 0.008–2.00 g were applied to the lateral plantar surface of hindpaw for 2–3 s with bending force using up-down method of Dixon [36]. A response was characterized as a brisk withdrawal to the stimulus applied, which included any abnormal exaggerated responses (e.g., biting and/or licking or extended elevation of the paw). The next smaller or larger filament is tested depending on the presence or absence of a positive response. The pattern of responses (maximum six responses) was recorded and converted to a 50% paw withdrawal threshold (PWT) to indicate the force of particular von Frey hair to which a mouse reacts in 50% of the presentations [37].

Cold Allodynia

Cold allodynia was measured by using acetone drop method [38]. Mice were habituated in elevated wire mesh platform in boxes as mentioned above. A drop of acetone was applied onto the lateral plantar surface of hindpaw using a 1-ml syringe without touching the skin. The duration of withdrawal response, licking, biting, or flinching was recorded for 1-min test period. Baseline values were measured on two alternate days before paclitaxel injections. Average value of six responses per mouse was calculated [32, 37, 39, 40].

Immunohistochemistry of Skin and Nerve Biopsies

On day 31 (endpoint of all behavior tests), deeply anesthetized mice were transcardially perfused with 4% PFA. Hindpaw skin corresponding to the von Frey filament test site and sciatic nerve were dissected, cryoprotected with 30% sucrose, and frozen in OCT (Tissue-Tek).

Intraepidermal Nerve Fibers (IENFs) Density Quantification

Thirty-micrometer-thick cryosections from hindpaw skin were immunostained with anti-protein gene product 9.5 (PGP9.5) antibodies (Ultraclone) that identified IENFs, and confocal images were obtained using Leica TCS SP5. The number of intraepidermal nerve fibers (IENFs) that crossed the dermal/epidermal junction into epidermis was quantified in five random fields from every fifth 30-μm-thick serial cryosections in each animal ($n = 5$ per group). The length (mm) of epidermis within each field was measured and calculated as IENF density (number of fibers/mm) [17, 35].

Myelin Basic Protein (MBP) Immunoreactivity Quantification

Four-micrometer-thick transverse sections of sciatic nerve were immunostained with anti-MBP antibodies (Abcam). Fluorescent images were taken to cover the whole transverse sectional area of sciatic nerve. The ImageJ software was used to quantify MBP immunoreactivity and measure the total area of nerve as described [41]. Data was represented as mean ± SEM of percentage of MBP immunoreactivity/total area of nerve [42].

Quantification of Axon Diameter and Demyelinated Axons

Sciatic nerves were dissected from below its trifurcation, first post-fixed in 2% glutaraldehyde and 2% PFA and subsequently in 2% osmium tetroxide. Sciatic nerves were dehydrated in gradient ethanol, infiltrated, and embedded with Spurr's resin. Semi-thin (300 nm) and ultra-thin (70 nm) transverse sections of sciatic nerves were prepared using an Ultracut UCT ultramicrotome (Leica). Semi-thin sections were fixed on Superfost™ Plus slides and stained with toluidine blue. Images were captured at 40× using an Axioplan 2 light microscope (Carl Zeiss) and axon diameter was measured by using analySIS® LS (Olympus Imaging). Degenerated axons leaves smaller myelin fragments termed "myelin ovoids" due to myelin sheath breakdown in-between the spaces of intact myelinated axons. Degenerated axons appear as either dark or dull colored dispersed nearby intact myelinated axons [43, 44]. Myelin ovoids (indicated by red arrows) were counted manually with the ImageJ software in each 100× image per mouse ($n = 3$ mice per group) and degenerating axon profile was presented as mean ± SEM.

Electron Microscopy

Ultra-thin sections of sciatic nerves were mounted on carbon coated 230-mesh copper grids and stained with lead citrate and 2% uranyl acetate. Myelinated and unmyelinated axons were imaged on a transmission electron microscopy (TEM) (FEI/Philips Tecnai 12 BioTWIN, TSS microscopy). The average diameter of mitochondria was measured along their short axis in 4–5 electron microscopy images per animal by the Image J software [43]. The number of unmyelinated axons was counted in 3–4 random images per mouse in each treatment group and normalized per 10,000 μm^2 as described previously [45].

Detection of Apoptosis

After 30 days of paclitaxel injection, apoptosis in lumbar 4, 5, and 6 (L4/5/6 DRGs) was detected by terminal deoxynucleotidyl transferase dUTP nick-end labeling (TUNEL) assay using the in situ apoptosis detection kit (Chemicon) according to the manufacturer's instruction [41]. Briefly, every fourth 5-μm-thick L4/5/6 DRG sections were treated with ice-cold 2:1 ethanol/acetic acid (*v*/*v*) followed by PBS wash before incubated with neuronal marker anti-PGP9.5 (Ultraclone) to identify neurons. DRG sections were then incubated with reaction buffer and terminal deoxynucleotidyl transferase at 37 °C. Stop/wash buffer was added to each sample and incubated with anti-digoxigenin fluorescein conjugate at room temperature. DRG sections were counter-stained with DAPI. Total number of TUNEL-positive cells overlapped with PGP9.5-positive cells and DAPI-stained nuclei were counted in each section (at least 10 sections per mouse). Representative images were captured at 40× magnifications using a Nikon Eclipse Ni-E fluorescence microscope.

Sensory Nerve Action Potential (SNAP) and Nerve Conduction Velocity (NCV)

Adult mice were deeply anesthetized with ketamine (100 mg/kg) and xylazine (10 mg/kg). The left hindpaw and tail base were shaved and wiped with ethanol. Body temperature of mice was maintained at 37 °C using the heating pad. Baseline values were recorded before paclitaxel injection. After injection, weekly sensory nerve action potential (SNAP) amplitudes and nerve conduction velocity (NCV) of caudal nerve were recorded (Blackrock microsystem, data acquisition set-up, USA). In general, recordings were sampled at 5 kHz, amplified, and passed through a band-pass filter of 10 and 250 Hz and filtered through a digital high-pass filter. Stimulating electrode was inserted at the tail base and the distance between the stimulating and recording electrodes was at least 5 cm. Grounding and reference electrodes were inserted in-between the stimulation and recording electrodes at least 5 mm apart. A square wave stimulus with supramaximal intensity for 0.2 ms duration was delivered at a frequency of 1 Hz using a stimulus isolator (Iso-flex; Israel) and Master 9 (AMPI, Israel). For each mouse, 50–60 stimuli were recorded and at least 20–30 peak-to-peak amplitudes and latencies per mouse were quantified using the Spike 2 software (Cambridge Electronic Design Limited, England). Data were presented as mean ± SEM for each group. SNAP amplitude was calculated as the difference between the maximum positive and negative deflections (peak to peak). NCV was calculated using peak latency and distance between the stimulating and recording electrode. Peak latency (ms) was measured from stimulating artifact to the peak of negative deflection of SNAP in biphasic response, while peak of initial positive deflection from baseline was used in triphasic response [46].

Western Blot Analysis

Western blot analysis of total protein extracts from L4/5/6 DRGs and whole sciatic nerves was performed 30 days after paclitaxel injection. DRGs and sciatic nerves were mechanically dissociate in lysis buffer and protein samples were separated on 4–12% NuPAGE Bis-Tris precast gel (Invitrogen) as described [21, 41]. Protein was transferred onto the PVDF membrane (Bio-Rad) and blocked with 5% (*w*/*v*) non-fat dry milk, incubated with anti-caspase 3 (Cell Signaling Technology), anti-RhoA (Santa Cruz Biotechnology Inc.), anti-phospho-cofilin (Cell Signaling Technology), and anti-GAPDH antibody (Santa Cruz Biotechnology Inc.) as loading control. Membrane was then washed and incubated with horseradish peroxidase-conjugated secondary antibodies,

washed and signals were detected by West Femto Maximum Sensitivity Substrate Kit (Thermo Scientific). Membrane was stripped and re-blotted with antibodies specific to total cofilin (Cell Signaling Technology). Band intensities were measured using the ImageJ software. RhoA levels were normalized to GAPDH. Cleaved caspase 3 and phospho-cofilin levels were first normalized to total caspase 3 and total cofilin levels, respectively, and then normalized to GAPDH.

Statistical Analysis

All the data were presented as mean ± SEM. Animal behavior data were analyzed by two-way ANOVA multiple comparison with post hoc Bonferroni's test. All other data were analyzed by Student's *t* test (2 groups) and 1-way ANOVA with post hoc Bonferroni's test (> 2 groups) where appropriate. All graphs were generated and statistically analyzed using the GraphPad Prism 6.0 software.

Results

Forced Expression of hHsp27 in DRG Neurons Reverses Paclitaxel-Induced Mechanical and Cold Allodynia

We first assess the protective effect of hHsp27 on primary DRG neurons since paclitaxel damaged sensory neurons in culture directly by affecting cytoskeleton arrangement [1]. We generated transgenic mice that hHsp27 is expressed postnatally in sensory neurons under neuronal-specific promoter Thy1.2 as described [21]. Here, we showed that forced expression of hHsp27 overcame the inhibitory effect of paclitaxel on axon growth in DRG neurons (Fig. 1a). Paclitaxel showed no effect on cell survival at 5–100 ng/ml of paclitaxel (Fig. 1b); however, we observed a significant cell death in LM mice (28.9 ± 9.9% of survival) when DRG neurons were treated with paclitaxel at higher dose (10 μg/ml) where most of the DRG neurons were protected in hHsp27 Tg mice (75.7 ± 4.5% of survival). For neurite outgrowth assay, we distinguished hHsp27-expressing neurons from non-hHsp27-expressing ones in the same DRG cultures prepared from hHsp27 Tg mice by immunostained with anti-hHsp27 antibody [21]. hHsp27-expressing neurons were protected from paclitaxel-induced neurite outgrowth inhibition significantly, when compared with littermate (LM) and non-hHsp27-expressing neurons at various doses ranged from 5 to 100 ng/ml in which the total neurite length was greatly reduced by 54–80% (Fig. 1c).

We next investigated the in vivo protective effect of hHsp27 by using animal model of paclitaxel-induced peripheral neuropathy in mice. To induce peripheral neuropathy, mice were intraperitoneally injected with paclitaxel (6 mg/ml) at the dose of 1 mg/kg on four alternating successive days (days 0, 2, 4, and 6) [47]. Analogous to CIPN patients, exposure of adult mice to paclitaxel induced sensory deficits such as mechanical and thermal allodynia (Fig. 2) [12, 17, 46, 47]. We assessed bilateral (both hindpaw) mechanical allodynia by using von Frey filament test during 1 month after paclitaxel injection on day 0 since paclitaxel produced a bilateral neuropathy [12, 15]. Values presented as average PWT from both hindpaws. LM mice treated with paclitaxel reduced the thresholds for mechanical stimuli to elicit a paw withdrawal response significantly starting on day 8 and was sustained for over 4 weeks. hHsp27 forced expression prevented the development of mechanical allodynia that hHsp27 Tg mice did not exhibit significant differences from the saline-treated control group (Fig. 2a).

Acetone-induced evaporative cooling that is commonly used to assess cold allodynia in CIPN mice [32, 33]. Increased responses after acetone application on both hindpaws were detected within 5 days in saline-treated mice and sustained for over a 30-day time course in paclitaxel-treated LM mice indicated that cold allodynia was rapidly developed. Strikingly, cold allodynia was not developed in hHsp27 Tg mice which maintained at baseline response levels throughout the study time course (Fig. 2b).

hHsp27 Protects Against Paclitaxel-Induced Degeneration of Afferent Nerve Fibers and Restores Sensory Nerve Action Potential

It has been well documented that reduction of IENF density resulting from terminal arbor degeneration, decrease in SNAP amplitude, and NCV are signatures of paclitaxel-induced damages to nociceptive neurons that is directly associated with the development of allodynia [12, 17, 46, 47]. We therefore performed histology and electrophysiology analysis to validate the neuroprotective effect of hHsp27 observed in behavioral tests. We quantified the number of IENFs in lateral hindpaw which is where the nerve endings of nociceptive neurons that innervate epidermis as well as primary mechanical allodynia testing site is located (Fig. 3a). Paclitaxel treatment reduced IENF density at the lateral hindpaw skin significantly by 60.5% on day 29 after paclitaxel treatment, in which persistent allodynia was evident in our behavior tests. Remarkably, IENFs were well preserved in hHsp27 Tg mice (76.07 ± 4.24) to a level comparable to saline-treated controls (83.57 ± 5.05) (Fig. 3b). Caudal nerve is composed of mainly sensory fibers (~ 80–90%) that SNAP analysis is widely used to assess electrophysiologically the extent of sensory neuropathy in CIPN animals [46–48]. In line with the behavior and IENF density studies, caudal SNAP amplitude recorded from hHsp27 Tg mice were restored to control levels while the SNAP values remained significantly lower in LM mice (Fig. 3c).

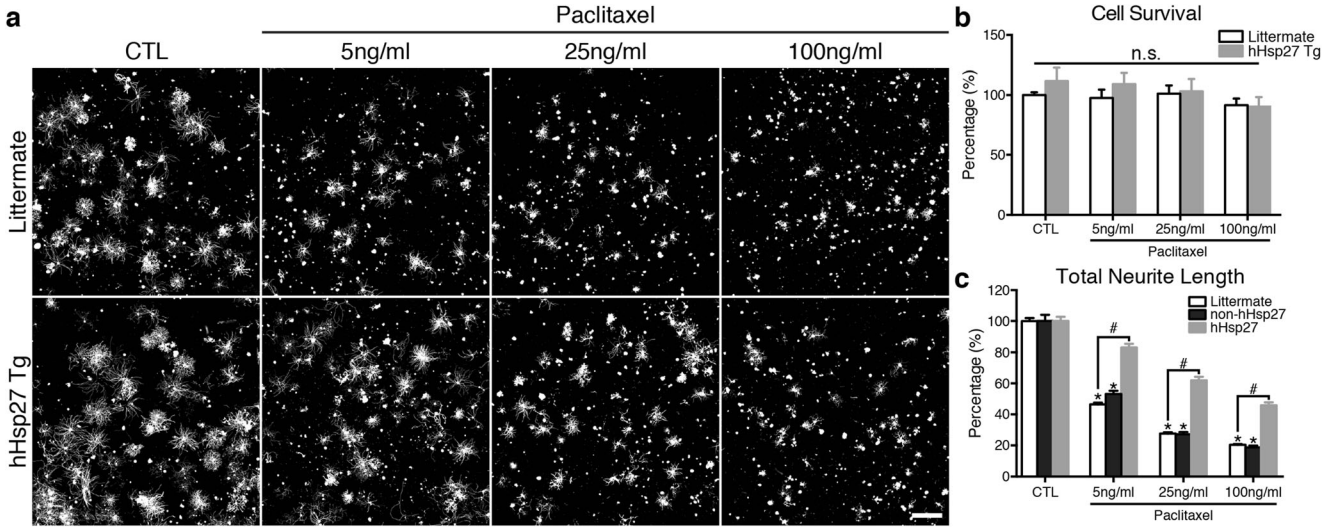

Fig. 1 Forced expression of hHsp27 protects adult dorsal root ganglion (DRG) neurons from paclitaxel-induced neurite outgrowth inhibition. Adult DRG neurons were grown on poly-D-lysine/laminin-coated 8-well slide chamber for 17 h to allow neurite extension. **a** Paclitaxel induced marked reduction in neurite extension from littermate (LM) DRG neurons in a dose-dependent manner. In contrast, DRG neurons from hHsp27 transgenic (Tg) mice possessed significantly longer neurites than LM mice, which illustrated the protective effects of hHsp27 on paclitaxel-induced neurite inhibition. 0.1% of Cremophor EL/ethanol (50:50) was used as vehicle control. Scale bar, 500 μm. **b** Paclitaxel treatment did not affect DRG neuron survival at all concentrations we tested, and DRG neurons remained healthy. **c** Average total neurite length per neuron was first measured using an automated program NeuroMath (Weizmann Institute of Science, Israel) and then normalized with respective controls in each individual experiment and expressed as percentage. Neurite outgrowth reduced dramatically at all concentrations in LM and non-hHsp27 DRG neurons. However, hHsp27 neurons exhibited significantly longer neurites when compared with LM and non-hHsp27 expressing neurons. Mean ± SEM of triplicates; $^{*}p < 0.05$, $^{\#}p < 0.05$, one-way ANOVA, followed by post hoc Bonferroni's test. CTL, control; n.s., not significant

hHsp27 Protects Myelinated and Unmyelinated Fibers Against Paclitaxel-Induced Degeneration

Paclitaxel induced substantial axonal degeneration and demyelination in CIPN patients [49]. Myelinated and unmyelinated sensory fibers are predominately damaged by chemotherapeutic agents including vinca alkaloids, platinum-based compounds, and taxanes such as paclitaxel in patients [50, 51] and rodents [43, 46, 52, 53]. Reduction of NCV has been reported in paclitaxel-treated patients which suggested the occurrence of peripheral nerve demyelination [54–56]. We first quantify the diameter of myelinated axons in toluidine blue-stained semi-thin cross sections of sciatic nerves 1 month after paclitaxel treatment (Fig. 4a). The number of large diameter axons (> 3 μm) was severely reduced by 54% in LM mice (Fig. 4b) accompanied by a reduction of average axon diameter (Fig. 4c), indicating that the loss of large diameter axons was completely prevented in hHsp27 Tg mice with average axon diameter returned to normal control levels. To examine axon demyelination, we quantify the number of demyelinated axons by identifying fragmented myelinated axons referred as "myelin ovoids" (see red arrows in Fig. 4a) [43, 44]. It clearly indicated that myelinated fibers in LM after treated with paclitaxel underwent segmentation of myelin into ovoids. In contrast, the number of myelin ovoids in hHsp27 Tg mice were remained the same as in the saline controls (Fig. 4d).

Myelin basic protein (MBP) is abundantly expressed in the myelin sheath [57], and the loss of MBP immunoreactivity indicates demyelination results in reduction of NCV [58]. Transverse sections of sciatic nerves were immunostained with anti-MBP antibodies (Fig. 5a), and MBP immunoreactivity was quantified in terms of percentage of intense MBP immunofluorescence per total field area measured [41, 42]. The extent of myelination was greatly reduced in LM mice as compared to hHsp27 Tg mice and controls (Fig. 5b). Caudal NCV recorded from hHsp27 Tg mice maintained largely at control levels although recording values remained significantly lower in LM mice throughout the study period (Fig. 5c). Consistent with these findings, ultrastructural study of sciatic nerves using TEM demonstrated a significant demyelination in LM-paclitaxel treatment group only, but the myelin was largely preserved in hHsp27 Tg mice as shown in Fig. S1.

To investigate the effect of paclitaxel on small unmyelinated fibers, we quantified unmyelinated axons in randomly selected fields per 10,000 μm^2 [45]. We observed a significant loss of small unmyelinated axons in paclitaxel-treated LM mice, while hHsp27 Tg protected small unmyelinated axons from degeneration as compared to saline controls (Fig. S2).

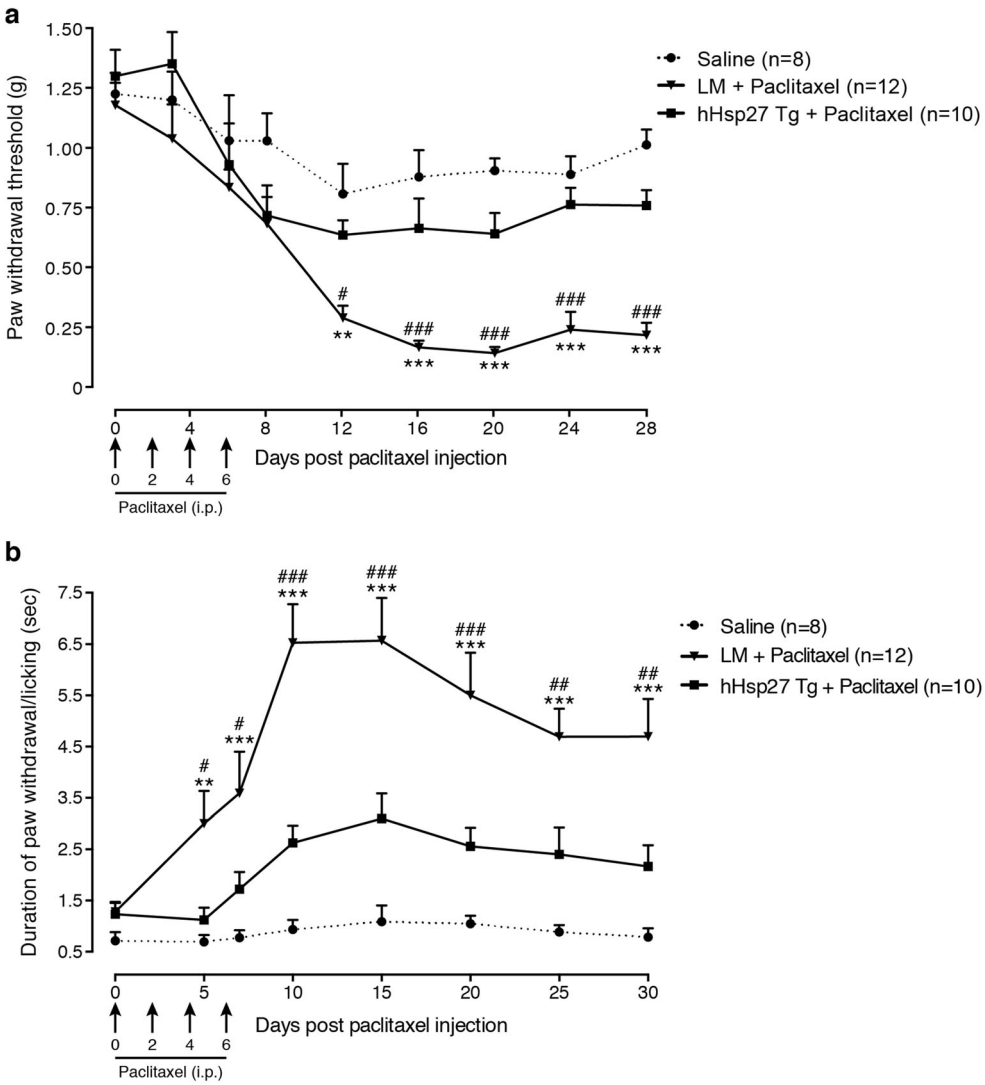

Fig. 2 Neuroprotective effects of hHsp27 in the mouse model of CIPN. In the first week, 1 mg/kg paclitaxel was injected intraperitoneally (i.p.) into adult hHsp27 transgenic (Tg) and their littermates (LM) mice on days 0, 2, 4, and 6 as indicated by arrows. LM mice were injected with saline as control. **a** Manual von Frey test was used to assess mechanical allodynia. LM developed significant mechanical allodynia as compared with both hHsp27 Tg mice and saline-treated mice 12 days after the first paclitaxel injection. **b** Acetone drop test was used to assess thermal allodynia. LM mice developed significant cold allodynia on day 5 after the first paclitaxel injection and sustained throughout the study period. In contrast, hHsp27 Tg mice did not exhibit significant cold allodynia when compared with controls. Mean ± SEM; $^{**}p < 0.01$ and $^{***}p < 0.001$ compared to saline control; $^{\#}p < 0.05$, $^{\#\#}p < 0.01$, and $^{\#\#\#}p < 0.001$ compared to hHsp27 Tg group, two-way ANOVA, followed by post hoc Bonferroni's test

hHsp27 Prevents Mitochondrial Swelling in Both Myelinated and Unmyelinated Fibers

Accumulating evidence indicates that strategies to ameliorate mitochondria dysfunction improve CIPN symptoms in animal studies [59–62]. Mitochondria insult due to chemotherapy induces mitochondrial swelling and vacuolation observed in peripheral nerves support the mitotoxicity hypothesis that axonal energy deficiency is one of the major causes of CIPN [52, 63, 64]. Ultrastructure morphometry analysis using TEM revealed prominent mitochondrial swelling in sciatic nerves of paclitaxel-treated LM mice, while hHsp27 Tg mice exhibited normal mitochondrial morphology in myelinated (Fig. 6a) and unmyelinated axons 30 days after paclitaxel treatment (Fig. 6b). After paclitaxel treatment, the diameter of mitochondria in both myelinated and unmyelinated axons was increased by 68% and 57%, respectively, when compared with saline control group. The diameter of mitochondria in hHsp27 Tg mice remained unchanged when compared with controls (Fig. 6c, d).

Hsp27 Exerts Anti-apoptotic Effect and Maintains Axon Integrity by Modulating Caspase 3 and RhoA Signaling Pathways

To further examine the underlying mechanism of hHsp27-induced protective effect on CIPN, we first quantified the numbers of DRG neurons undergoing apoptosis by TUNEL assay 30 days after paclitaxel treatment (Fig. 7a). Chemotherapy agents such as cisplatin and oxaliplatin have been known to induce apoptotic cell death in DRG neurons in vitro and in vivo [44, 65]. Consistent with a recent study, demonstrating for the first time that paclitaxel induced apoptotic cell death in DRG neurons [66], we detected a significant higher number of TUNEL-positive cells in LM mice than hHsp27 Tg mice in DRGs (Fig. 7b). Next, we examined the

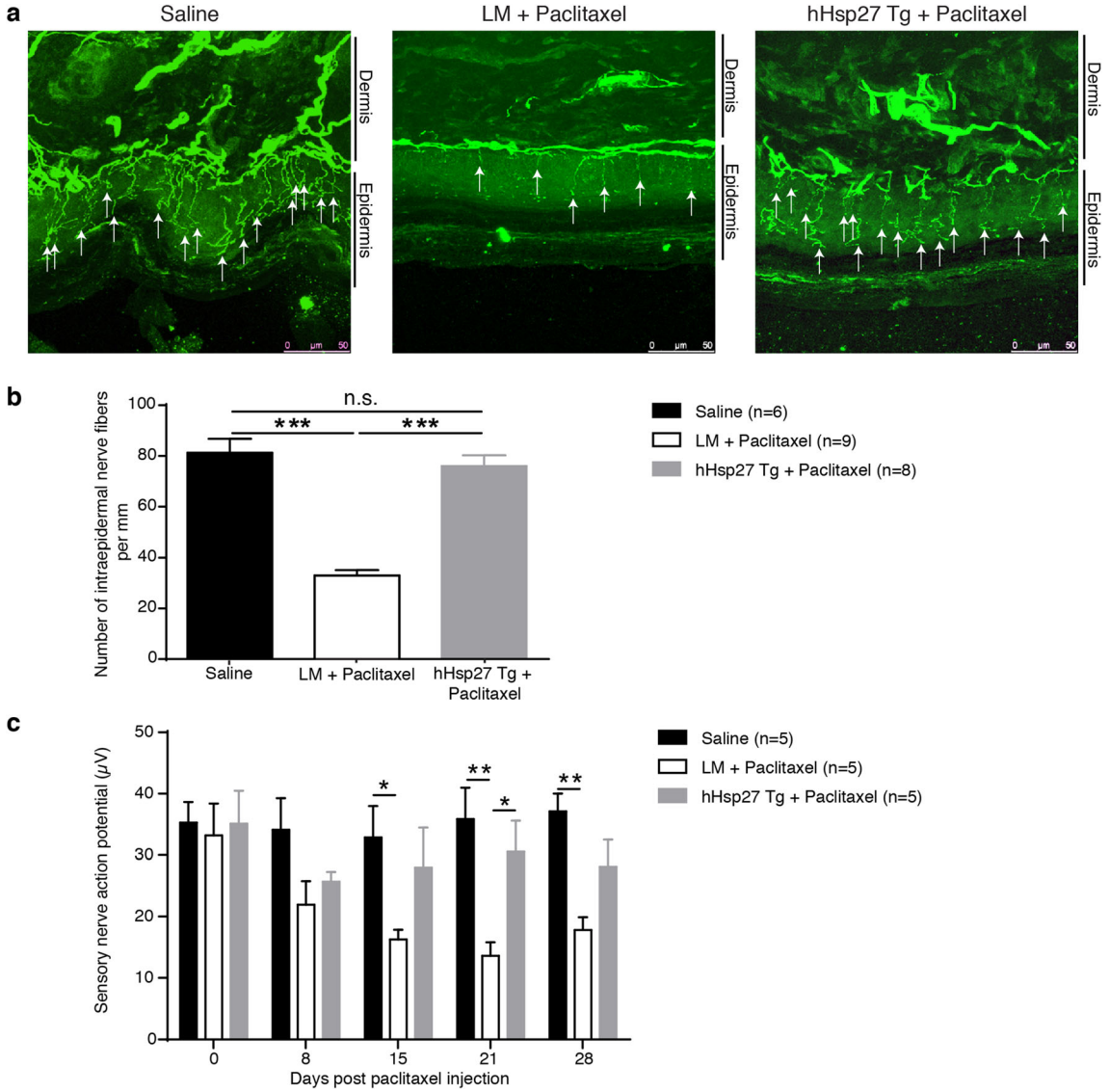

Fig. 3 hHsp27 protects sensory nerve fibers from paclitaxel-induced peripheral neuropathy and restores sensory nerve action potential (SNAP). **a** The confocal images showed that intraepidermal nerve fibers (IENFs) (indicated by white arrows) immunostained for PGP9.5 in lateral hindpaws where the primary mechanical allodynia testing site is located. Skin biopsy was taken 30 days after paclitaxel treatment. Severe loss of IENFs was evident in LM mice after paclitaxel treatment while IENFs were largely preserved in hHsp27 mice. Scale bar, 50 μm. **b** IENF density was quantified and reduced significantly in LM-treated mice only in which persistent allodynia was evident in behavior tests. ***$p < 0.0001$, one-way ANOVA, followed by post hoc Bonferroni's test (5 fields of every fifth section, 5 sections per mouse were quantified). **c** Electrophysiological recording from caudal nerve after paclitaxel treatment was performed on weekly basis to monitor CIPN progression. Reduced SNAP amplitudes were only observed in LM mice after paclitaxel treatment. SNAP amplitudes were comparable between hHsp27 and control mice. Mean ± SEM; *$p < 0.05$, **$p < 0.01$, two-way ANOVA, followed by post hoc Bonferroni's test. n.s., not significant

activation of caspase family member, caspase 3, which is the farthest downstream effector in the apoptotic cascades. In line with the TUNEL assay results, strong activation of caspase 3 was detected by Western blot in paclitaxel-treated LM mice only, and hHsp27 exerted its anti-apoptotic effect by inhibiting caspase 3 activation in DRGs taken 30 days after paclitaxel treatment (Fig. 7c).

Finally, we investigated the association of axon integrity signaling pathway such as RhoA and its downstream effector cofilin with the development of CIPN. Accumulating evidence suggests that RhoA signaling pathway is strongly linked to allodynic responses in animal model of nerve injury, inflammatory pain, and CIPN [67–70]. We therefore reasoned that forced expression of hHsp27 might exert its anti-allodynic effects via the modulation of RhoA/cofilin signaling pathway. Total protein was extracted from L4/5/6 DRGs that supply the sciatic nerves directly and from the whole sciatic nerves for Western blot analysis. In LM mice, paclitaxel induced cofilin phosphorylation resulting from RhoA activation in DRG neurons (RhoA 1.43 ± 0.10-fold, pCofilin 3.06 ± 0.40-fold) (Fig. 8a) and its

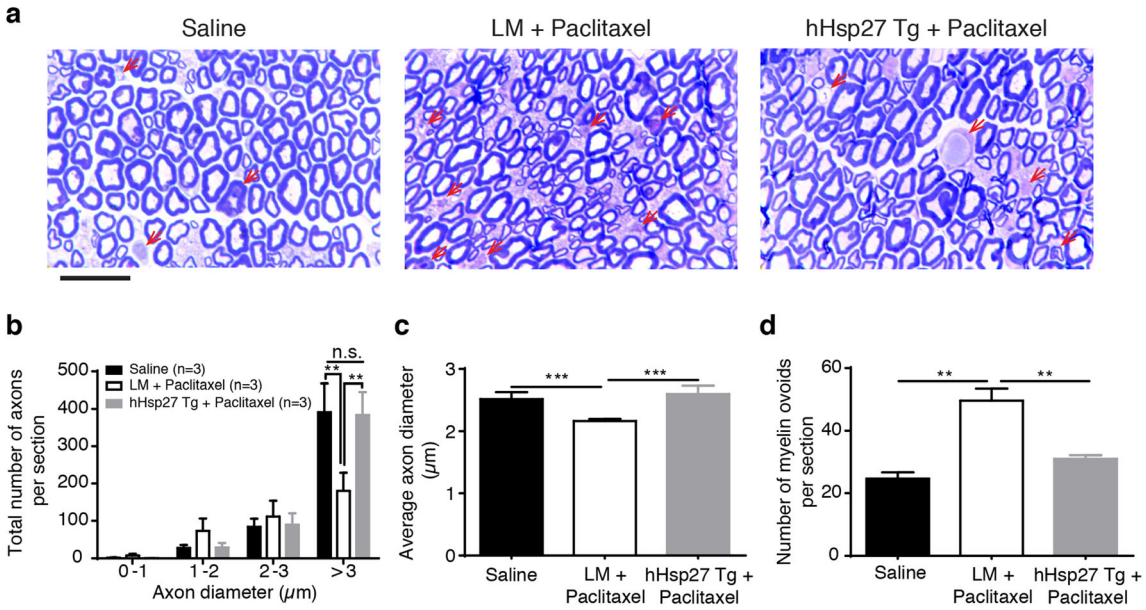

Fig. 4 hHsp27 protects large diameter myelinated fibers against paclitaxel-induced degeneration. **a** Toluidine blue-stained semi-thin sections (300 nm) of sciatic nerves 30 days after paclitaxel treatment. Myelin ovoids were indicated by red arrows. Scale bar, 10 μm. **b** The number of large diameter axons in hHsp27 mice were preserved, when compared with LM mice. $^{**}p < 0.01$, two-way ANOVA, followed by post hoc Bonferroni's test. **c** Paclitaxel-treated LM mice showed significant reduction of mean axon diameter when compared with hHsp27 Tg and control mice. In **b** and **c**, 328–600 axons were counted per mouse in each treatment group. **d** Number of demyelinated axons was quantified by identifying fragmented myelinated axons. Paclitaxel-treated LM mice underwent segmentation of myelin into ovoids. In contrast, the number of myelin ovoids were remained the same as between saline control and hHsp27 Tg mice. Mean ± SEM; $^{**}p < 0.01$, $^{***}p < 0.001$, one-way ANOVA, followed by post hoc Bonferroni's test. n.s., not significant

axons in sciatic nerves (RhoA 1.51 ± 0.11-fold, pCofilin 2.13 ± 0.30-fold) (Fig. 8b). It indicates that administration of paclitaxel induced activation of RhoA/cofilin signaling pathway, which might account for mechanical and thermal allodynia observed in paclitaxel-treated animals. In contrast, protein expression levels of RhoA and cofilin phosphorylation in hHsp27 Tg mice were significantly reduced compared with age-matched LM mice treated with paclitaxel and were comparable between hHsp27 Tg and saline-treated mice (Fig. 8). Taken together, our results support the neuroprotective role of Hsp27 in CIPN through inhibition of RhoA/cofilin signaling pathway.

Discussion

Chemotherapy is effective in treating cancer; however, peripheral neuropathy is often the results. CIPN is one of the most severe and unpredictable side effects of modern anti-cancer drugs including paclitaxel. CIPN in human is mainly characterized by sensory disturbances (numbness, tingling, and allodynia), which affects patient's quality of life results in dose reductions of life-saving therapies and eventually discontinuation of chemotherapy. In most cases, CIPN is not reversible and can be permanent even if the symptoms are partially resolved after discontinuation of treatment. There is currently no effective treatment to prevent or reverse CIPN. Here, we show that Hsp27 overexpression completely reverses the major symptoms of paclitaxel-induced peripheral neuropathy including mechanical and cold allodynia by targeting major signaling pathways in axon integrity.

A growing body of evidence supports that paclitaxel induces not only axonal degeneration but also neuronal cell death. In primary dissociated DRG cultures prepared from embryonic (E) day 15 rats, paclitaxel induced neuronal cell death at higher dose (~ 10 μM) and reduced neurite outgrowth at lower dose of paclitaxel (~ 10 nM) [71]. Another study using similar doses reported that paclitaxel induced apoptotic cell death in cultured E14 rat DRG neurons detected by TUNEL assay as well as reduction of neurite outgrowth dramatically by 50% [72]. A recent animal study demonstrated for the first time that paclitaxel induced apoptotic cell death in DRG neurons along with increased activation of caspase 3 expression, due largely to the activation of fractalkine (CX3CL1). Administration of neutralizing antibodies against CX3CL1 blocked paclitaxel-induced infiltration of macrophage into the DRGs and partially reduced mechanical allodynia, but the treated animals fail to return to baseline levels [66]. Several studies demonstrated modulation of innate immune cells; glial-derived cytokines such as TNF-α, IL-1β, and IL-10; neuroinflammation in the spinal cord; and alternation in glutamatergic signaling pathways, which underlie the development of paclitaxel-induced peripheral neuropathy.

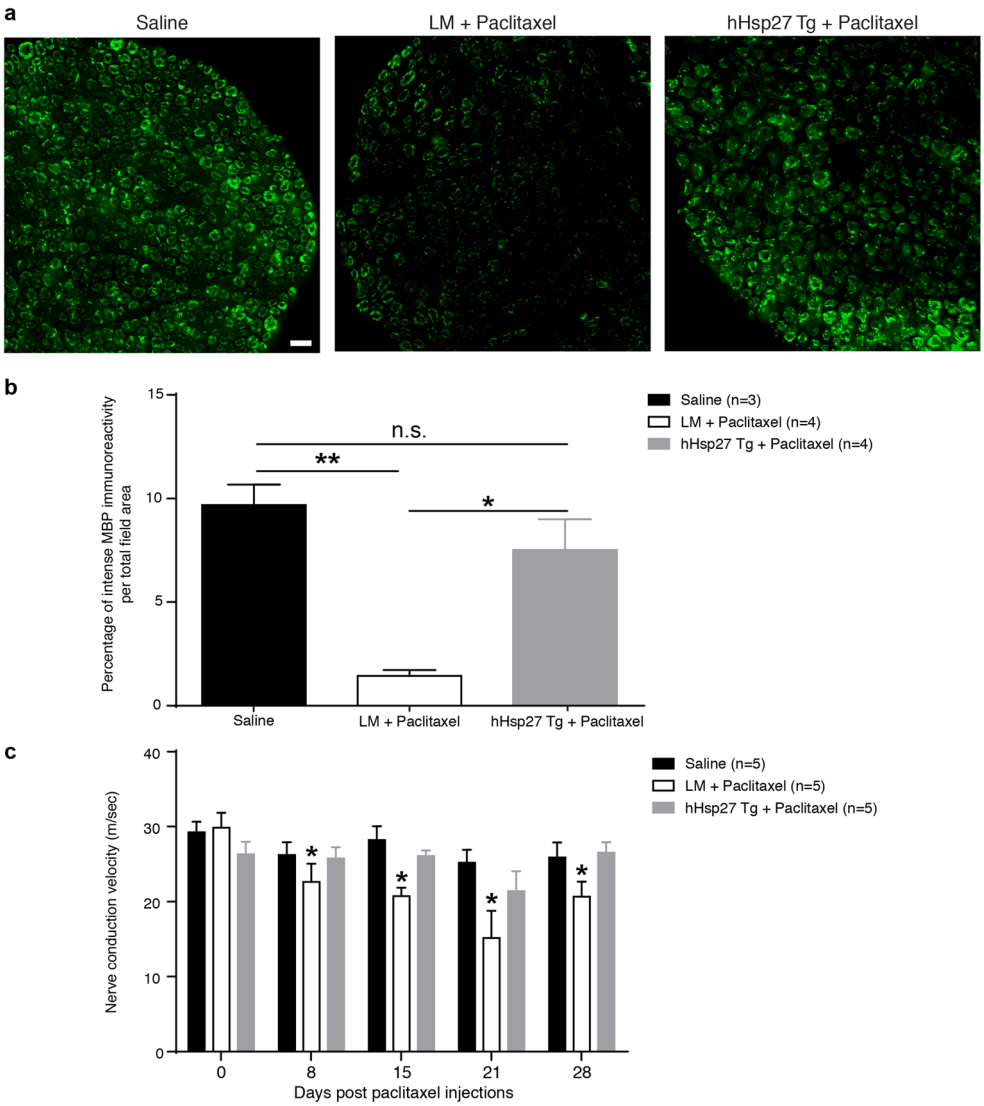

Fig. 5 hHsp27 prevents demyelination of axons in sciatic nerves after paclitaxel treatment. **a** Transverse sections of sciatic nerves (4-μm-thick) were immunostained for myelin basic protein (MBP) 30 days after paclitaxel injection. Scale bar, 10 μm. **b** MBP immunoreactivity was quantified in terms of percentage of intense MBP immunofluorescence per total field area measured. Paclitaxel induced significant reduction of myelination in LM mice as compared to hHsp27 Tg mice and controls. $*p < 0.05$, $**p < 0.01$, one-way ANOVA, followed by *post hoc* Bonferroni's test. **c** In LM mice, nerve conduction velocity (NCV) of caudal nerve decreased significantly 1 week after the first injection throughout the study period of 28 days, while the NCV recorded from hHsp27 Tg mice maintained at control levels. Mean ± SEM; $*p < 0.05$, two-way ANOVA, followed by post hoc Bonferroni's test. n.s., not significant

Paclitaxel induced significant infiltration of 14 different types of immune cells such as macrophages, helper and cytotoxic T cells, leukocytes, monocytes, antigen presenting cells, and neutrophils in DRGs. Neutralizing antibody specific to pro-inflammatory $CD8^+$ T cells ameliorated paclitaxel-induced mechanical allodynia [73]. Spinal cord microglia activation has long been closely linked with development of neuropathic and inflammatory pain in mice. Increased levels of caspase 6 were detected in cerebrospinal fluid after inflammation. Strong expression of caspase 6 was observed in dorsal horn glial cell in laminae I/II and c-fiber axonal terminal originated from nociceptive DRG neurons. The c-fiber axonal terminal was in close proximity with microglia where caspase 6 activation regulated microglial TNF-α release. Intrathecal injection of minocycline (microglial inhibitor) or TNF-α neutralizing antibody reduced pain hypersensitivity in an animal model of inflammatory pain [74, 75]. However, the major contributor to paclitaxel-induced peripheral neuropathy remains controversial due to the difficulty of identifying cell population responsible for the development of slowly advancing peripheral neuropathy.

Hsp27 has been shown to prevent activation of caspase 3 in injured DRG neurons [76] and accelerate axonal regeneration [21]. Paclitaxel induces apoptosis by increasing pro-apoptotic protein cytochrome c release primarily through the opening of mitochondrial permeability transition pore (mPTP) as a result of calcium dysregulation and mitochondrial dysfunction [13, 36, 52, 77]. Paclitaxel is also known to target microtubules and β-tubulin, thereby interfering with microtubule dynamics [1, 78]. Growing evidence suggests that modulation of actin filament dynamics via RhoA/LIMK/cofilin signaling pathways in different animal models of neuropathic pain such as CIPN could be a potential molecular target. Elevated levels of RhoA and phosphorylation of its effectors LIM domain kinase (LIMK) and cofilin have been associated with the development of inflammatory pain hypersensitivity [79, 80], chronic

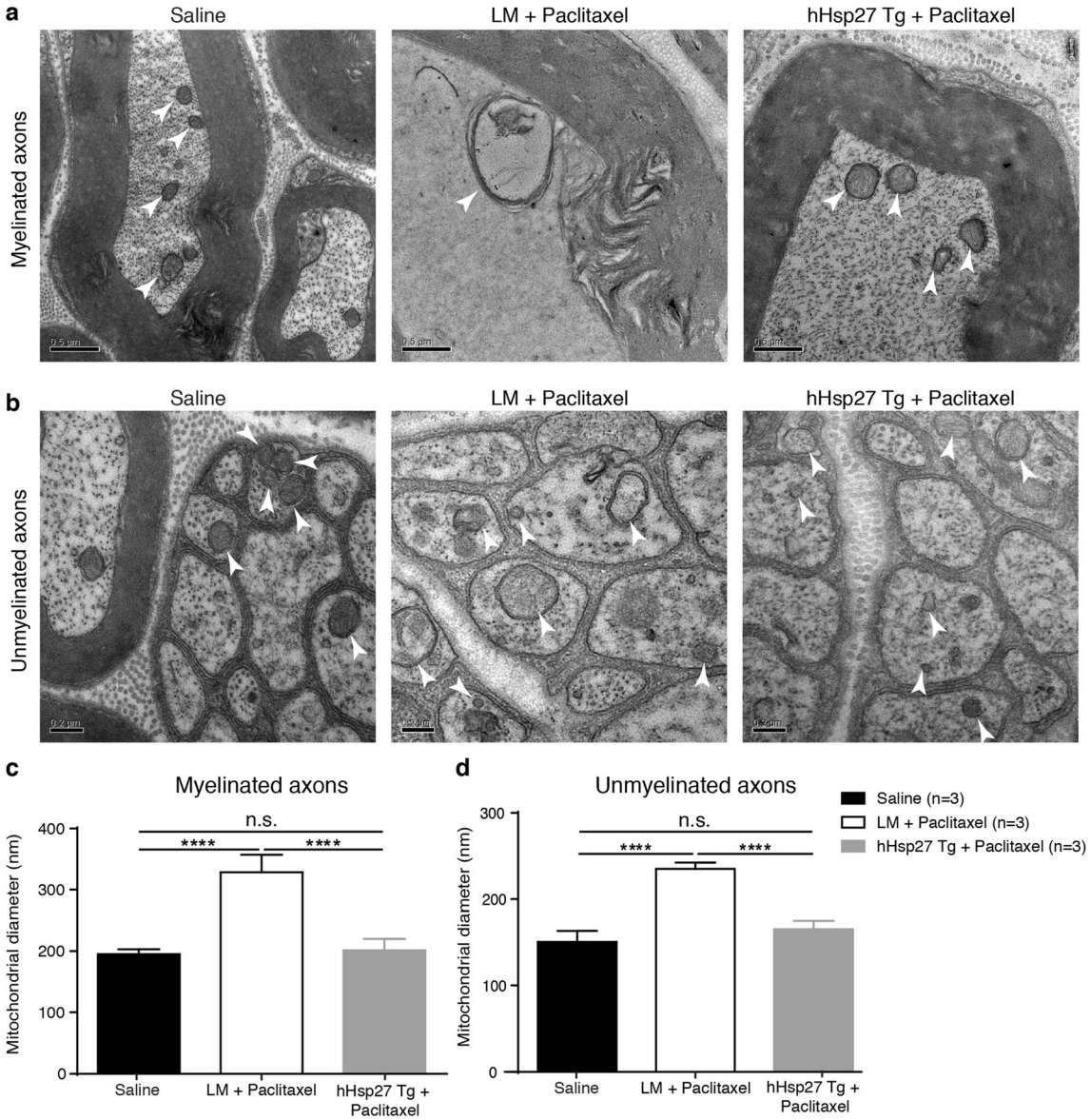

Fig. 6 hHsp27 prevents mitochondrial swelling in both myelinated and unmyelinated fibers. **a**, **b** Ultrastructure morphometry analysis using transmission electron microscopy revealed that increased mitochondrial swelling was observed in myelinated axons and unmyelinated axons 30 days after paclitaxel treatment in littermate (LM) mice only. White arrowheads indicated mitochondria. Scale bar, 0.5 μm (myelinated) and 0.2 μm (unmyelinated). **c**, **d** Quantification of mitochondrial diameter showed significant mitochondrial swelling in both myelinated axons and unmyelinated axons in LM mice, when compared with hHsp27 Tg and control mice. Mean ± SEM; $****p < 0.0001$, two-way ANOVA, followed by post hoc Bonferroni's test. n.s., not significant

neuropathic pain [70], and CIPN [67, 68]. Activation of RhoA was detected shortly after intraplantar administration of inflammatory agents, and RhoA inhibition partially rescued mechanical and thermal hyperalgesia through the inhibition of cofilin phosphorylation [79, 80]. In a rat model of chronic constriction injury (CCI), upregulation of RhoA led to increased phosphorylation of LIMK and cofilin was detected at day 7 and sustained until day 21 after nerve injury, demonstrating a strong correlation between RhoA activation and the development of neuropathic pain. Potential therapeutic agents that aimed to block activation of ROCK (Y-27632) and to dephosphorylate cofilin (Tat-S3 peptides), which attenuated mechanical allodynia and thermal hyperalgesia in CCI-injured rats. However, none of these animals returned to baseline levels after treated with either Y-27632 or Tat-S3 peptides [70]. In a mouse model of CIPN, cisplatin induced mechanical allodynia 6 weeks after injection. Administration of LM11A-31 targeting $p75^{NTR}$, the upstream effector for RhoA, partially protected the mice from developing allodynic responses 10 weeks after cisplatin injection [67].

Our previous study demonstrated that mouse homolog of Hsp27 (mHsp25) co-localized with F-actin at the tips of DRG

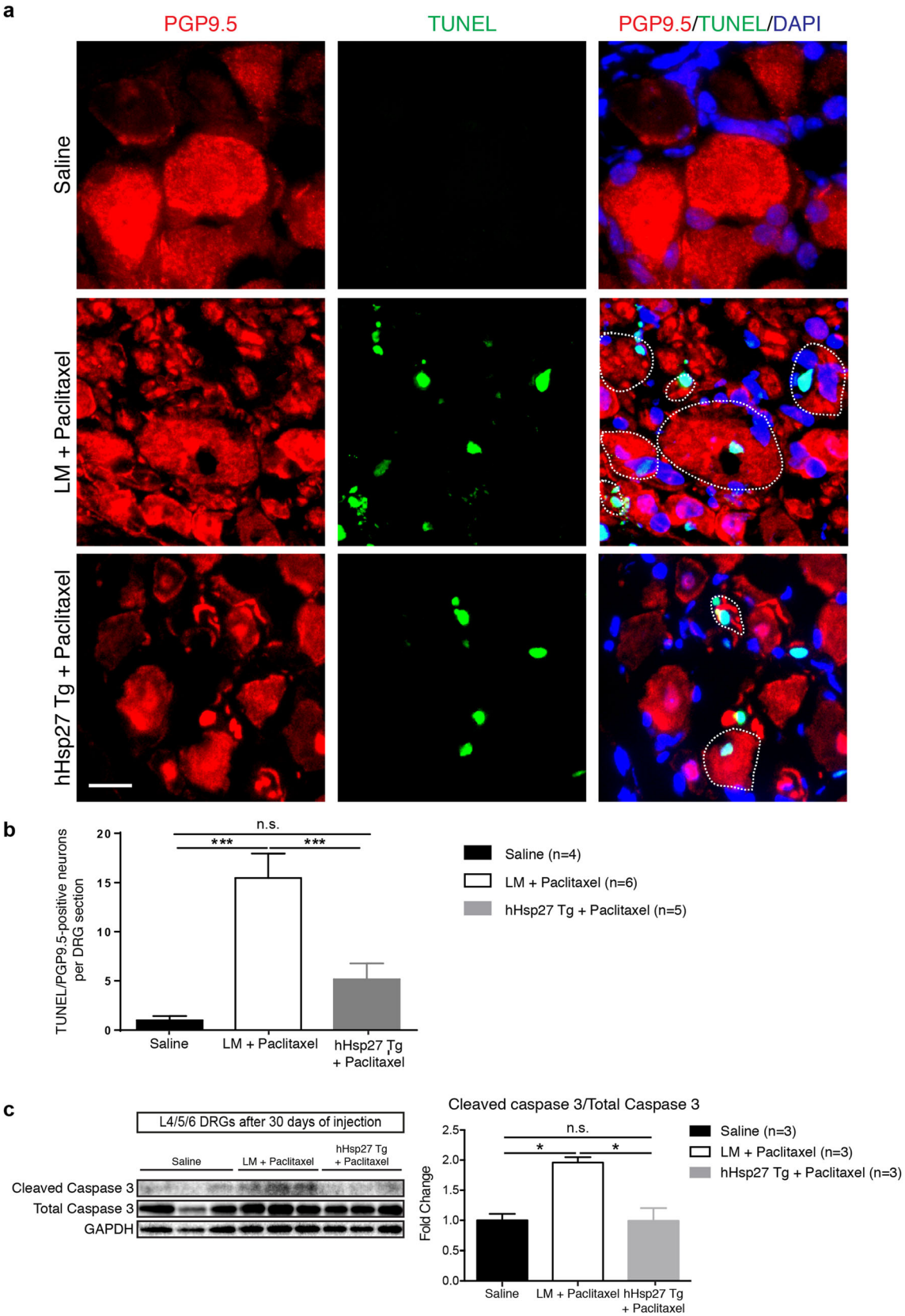

neuronal growth cones to facilitate neurite outgrowth results in accelerated axonal regeneration and promoted sensory and motor functional recovery after peripheral nerve injury [21]. Recent studies suggest that the growth promoting effect of

◀ **Fig. 7** hHsp27 protects DRG neurons against paclitaxel-induced apoptosis. **a** DRGs were harvested 30 days after paclitaxel treatment. TUNEL assay was performed on 5 μm-thick DRG cryosections. Scale bar, 20 μm. **b** Increased number of TUNEL/PGP9.5-positive apoptotic neurons were detected in paclitaxel-treated LM but not in hHsp27 Tg and control mice. TUNEL/PGP9.5-positive cells overlapped with DAPI-stained nuclei were counted in each section as outlined by white dotted line in **a** (at least 10 alternate sections per mouse). ***$p < 0.001$, one-way ANOVA, followed by post hoc Bonferroni's test. **c** Western blot analysis of cleaved caspase 3 expression in L4/5/6 DRG neurons after 30 days of paclitaxel treatment. Bar graph showed normalized fold change of cleaved caspase 3 protein expression. Band intensities of cleaved caspase 3 were measured and first normalized to total caspase 3 and then normalized to GAPDH as loading control. Mean ± SEM; *$p < 0.05$, one-way ANOVA, followed by post hoc Bonferroni's test. n.s., not significant

Hsp27 could be due, at least in part, to the inhibition of RhoA activity. RhoA is well known in regulating cytoskeletal dynamic in growth cone. Chemorepulsive secreted protein semaphorin 3a induced activation of RhoA and actin cytoskeleton rearrangement resulting in growth cone collapse [81]. In contrast, p53 and p21 prevent growth cone collapse through RhoA inactivation [82, 83]. In rat cortical neurons, overexpression of Hsp27 promoted neurite outgrowth on inhibitory substrate Nogo-66. Wild-type neurons cultured on Nogo-66 exhibited reduced neurite outgrowth along with high RhoA activity. RhoA activity in Hsp27-overexpressing neurons was markedly reduced by modulating the GTPase activity [84]. In the current study, we showed that forced expression of hHsp27 prevented apoptosis and preserved axon integrity results in reversing allodynic responses in paclitaxel-treated hHsp27 Tg mice. We further demonstrated that hHsp27 exerted its anti-apoptotic function by inactivating caspase 3 activity and maintained axon integrity by RhoA and its downstream effectors inactivation. Neuronal cell death, loss of intraepidermal nerve fibers, and aberrant demyelination are

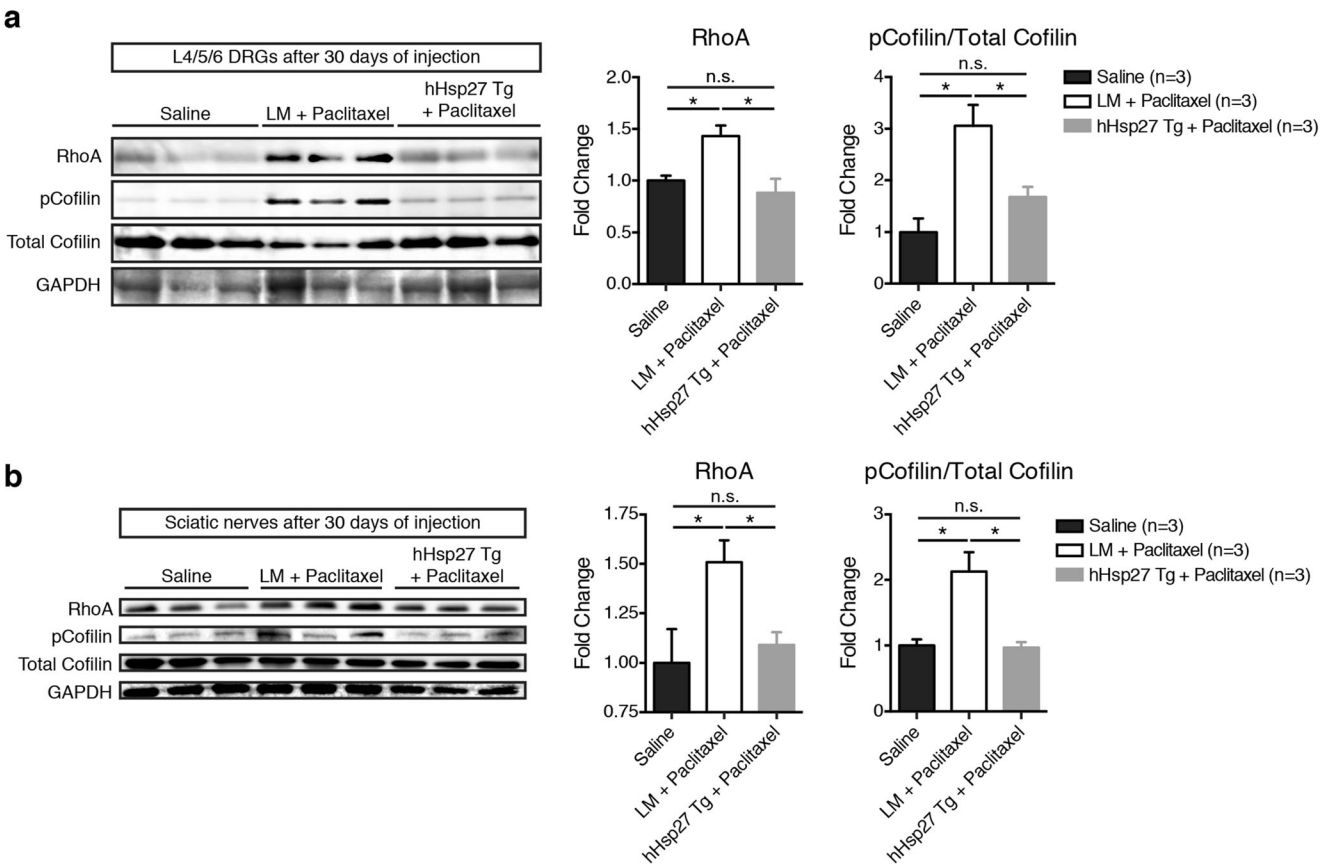

Fig. 8 Forced expression of hHsp27 inhibits paclitaxel-induced RhoA/cofilin activation in DRGs and sciatic nerves. L4/5/6 DRGs and whole sciatic nerves were harvested 30 days after paclitaxel injection, and protein lysate were subjected to Western blot analysis of RhoA/cofilin. **a** Paclitaxel induced robust increase in RhoA protein expression and phosphorylation of cofilin in L4/5/6 DRG neurons from LM mice, indicating activation of RhoA/cofilin signaling pathway. In contrast, activation of RhoA/cofilin was inhibited as the protein expression levels of RhoA and phosphorylated cofilin (pCofilin) in DRGs from paclitaxel-treated hHsp27 Tg were comparable to controls. **b** Activation of RhoA/cofilin signaling pathway was also detected in sciatic nerves of LM mice. The expression levels of RhoA and pCofilin were markedly reduced in paclitaxel-treated hHsp27 Tg mice. Band intensities of RhoA were measured and normalized to GAPDH as loading control. Band intensities of pCofilin were measured and first normalized to total cofilin, and then normalized to GAPDH. Bar graphs showed normalized fold change of RhoA/pCofilin protein expression. Mean ± SEM; *$p < 0.05$, one-way ANOVA, followed by post hoc Bonferroni's test. n.s., not significant

key features of paclitaxel-induced peripheral neuropathy. We therefore believe that Hsp27 could provide insight into the development of therapeutic approaches to CIPN. Future studies will be required to identify small molecules that activate key signaling pathways of Hsp27 by microarray and bioinformatics analysis. A recent study successfully identified a small molecule which promoted optic nerve regeneration using bioinformatics analysis [85].

Acknowledgements This work is supported in part by GRF grants from The Research Grant Council of the Hong Kong Special Administrative Region Government (CityU 11100015 and CityU 11100417), and the Health and Medical Research Fund, Food and Health Bureau, Hong Kong Special Administrative Region Government (05160126) award to Chi Ma.

Authors' Contributions VC carried out the neurobehavioral assessment, in vivo electrophysiological recording, immunohistochemistry of skin and nerve biopsies, electron microscopy, TUNEL assay, and Western blot analysis for cleaved caspase 3 protein expression. NPBA performed in vitro DRG culture analysis and Western blot analysis for RhoA/cofilin activation. GK validated and standardized SNAP and NCV recording. CHEM conceived the project, designed the study, and wrote the manuscript with inputs from all authors. All authors read and approved the final manuscript.

Compliance with Ethical Standards

Conflict of Interest The authors declare that they have no conflict of interest.

References

1. Au NP, Fang Y, Xi N, Lai KW, Ma CH (2014) Probing for chemotherapy-induced peripheral neuropathy in live dorsal root ganglion neurons with atomic force microscopy. Nanomedicine 10(6):1323–1333
2. Jaggi AS, Singh N (2011) Mechanisms in cancer-chemotherapeutic drugs-induced peripheral neuropathy. Toxicology 291(1–3):1–9
3. Pachman DR, Barton DL, Watson JC, Loprinzi CL (2011) Chemotherapy-induced peripheral neuropathy: prevention and treatment. Clin Pharmacol Ther 90(3):377–387
4. Dougherty PM, Cata JP, Cordella JV, Burton A, Weng HR (2004) Taxol-induced sensory disturbance is characterized by preferential impairment of myelinated fiber function in cancer patients. Pain 109(1–2):132–142
5. Windebank AJ, Grisold W (2008) Chemotherapy-induced neuropathy. J Peripher Nerv Syst 13(1):27–46
6. Verstappen CC, Koeppen S, Heimans JJ, Huijgens PC, Scheulen ME, Strumberg D, Kiburg B, Postma TJ (2005) Dose-related vincristine-induced peripheral neuropathy with unexpected off-therapy worsening. Neurology 64(6):1076–1077
7. Rowinsky EK, Chaudhry V, Cornblath DR, Donehower RC (1993) Neurotoxicity of Taxol. J Natl Cancer Inst Monogr 15:107–115
8. Michaud LB, Valero V, Hortobagyi G (2000) Risks and benefits of taxanes in breast and ovarian cancer. Drug Saf 23(5):401–428
9. Jordan MA, Wilson L (2004) Microtubules as a target for anticancer drugs. Nat Rev Cancer 4(4):253–265
10. Lee JJ, Swain SM (2006) Peripheral neuropathy induced by microtubule-stabilizing agents. J Clin Oncol 24(10):1633–1642
11. Hilkens PH, ven den Bent MJ (1997) Chemotherapy-induced peripheral neuropathy. J Peripher Nerv Syst 2(4):350–361
12. Siau C, Xiao W, Bennett GJ (2006) Paclitaxel- and vincristine-evoked painful peripheral neuropathies: loss of epidermal innervation and activation of Langerhans cells. Exp Neurol 201(2):507–514
13. Wang MS, Davis AA, Culver DG, Wang Q, Powers JC, Glass JD (2004) Calpain inhibition protects against Taxol-induced sensory neuropathy. Brain 127(Pt 3):671–679
14. Callizot N, Andriambeloson E, Glass J, Revel M, Ferro P, Cirillo R, Vitte PA, Dreano M (2008) Interleukin-6 protects against paclitaxel, cisplatin and vincristine-induced neuropathies without impairing chemotherapeutic activity. Cancer Chemother Pharmacol 62(6):995–1007
15. Smith SB, Crager SE, Mogil JS (2004) Paclitaxel-induced neuropathic hypersensitivity in mice: responses in 10 inbred mouse strains. Life Sci 74(21):2593–2604
16. Boyette-Davis J, Dougherty PM (2011) Protection against oxaliplatin-induced mechanical hyperalgesia and intraepidermal nerve fiber loss by minocycline. Exp Neurol 229(2):353–357
17. Boyette-Davis J, Xin W, Zhang H, Dougherty PM (2011) Intraepidermal nerve fiber loss corresponds to the development of taxol-induced hyperalgesia and can be prevented by treatment with minocycline. Pain 152(2):308–313
18. Tatsushima Y, Egashira N, Kawashiri T, Mihara Y, Yano T, Mishima K, Oishi R (2011) Involvement of substance P in peripheral neuropathy induced by paclitaxel but not oxaliplatin. J Pharmacol Exp Ther 337(1):226–235
19. Pan YA, Misgeld T, Lichtman JW, Sanes JR (2003) Effects of neurotoxic and neuroprotective agents on peripheral nerve regeneration assayed by time-lapse imaging in vivo. J Neurosci 23(36):11479–11488
20. Vuorinen VS, Roytta M (1990) Taxol-induced neuropathy after nerve crush: long-term effects on regenerating axons. Acta Neuropathol 79(6):663–671
21. Ma CH, Omura T, Cobos EJ, Latremoliere A, Ghasemlou N, Brenner GJ, van Veen E, Barrett L et al (2011) Accelerating axonal growth promotes motor recovery after peripheral nerve injury in mice. J Clin Invest 121(11):4332–4347
22. Lavoie JN, Gingras-Breton G, Tanguay RM, Landry J (1993) Induction of Chinese hamster HSP27 gene expression in mouse cells confers resistance to heat shock. HSP27 stabilization of the microfilament organization. J Biol Chem 268(5):3420–3429
23. Stetler RA, Cao G, Gao Y, Zhang F, Wang S, Weng Z, Vosler P, Zhang L et al (2008) Hsp27 protects against ischemic brain injury via attenuation of a novel stress-response cascade upstream of mitochondrial cell death signaling. J Neurosci 28(49):13038–13055
24. Huot J, Houle F, Spitz DR, Landry J (1996) HSP27 phosphorylation-mediated resistance against actin fragmentation and cell death induced by oxidative stress. Cancer Res 56(2):273–279
25. Lavoie JN, Lambert H, Hickey E, Weber LA, Landry J (1995) Modulation of cellular thermoresistance and actin filament stability accompanies phosphorylation-induced changes in the oligomeric structure of heat shock protein 27. Mol Cell Biol 15(1):505–516
26. Pichon S, Bryckaert M, Berrou E (2004) Control of actin dynamics by p38 MAP kinase - Hsp27 distribution in the lamellipodium of smooth muscle cells. J Cell Sci 117(Pt 12):2569–2577
27. Benndorf R, Hayess K, Ryazantsev S, Wieske M, Behlke J, Lutsch G (1994) Phosphorylation and supramolecular organization of murine small heat shock protein HSP25 abolish its actin polymerization-inhibiting activity. J Biol Chem 269(32):20780–20784
28. Chaudhuri S, Smith PG (2008) Cyclic strain-induced HSP27 phosphorylation modulates actin filaments in airway smooth muscle cells. Am J Respir Cell Mol Biol 39(3):270–278

29. Tezel G, Wax MB (2000) The mechanisms of hsp27 antibody-mediated apoptosis in retinal neuronal cells. J Neurosci 20(10): 3552–3562
30. Caroni P (1997) Overexpression of growth-associated proteins in the neurons of adult transgenic mice. J Neurosci Methods 71(1):3–9
31. Torres L, Danver J, Ji K, Miyauchi JT, Chen D, Anderson ME, West BL, Robinson JK et al (2016) Dynamic microglial modulation of spatial learning and social behavior. Brain Behav Immun 55:6–16
32. Flatters SJ, Bennett GJ (2004) Ethosuximide reverses paclitaxel- and vincristine-induced painful peripheral neuropathy. Pain 109(1–2):150–161
33. Polomano RC, Mannes AJ, Clark US, Bennett GJ (2001) A painful peripheral neuropathy in the rat produced by the chemotherapeutic drug, paclitaxel. Pain 94(3):293–304
34. Griffin RS, Costigan M, Brenner GJ, Ma CH, Scholz J, Moss A, Allchorne AJ, Stahl GL et al (2007) Complement induction in spinal cord microglia results in anaphylatoxin C5a-mediated pain hypersensitivity. J Neurosci 27(32):8699–8708
35. Korngut L, Ma CH, Martinez JA, Toth CC, Guo GF, Singh V, Woolf CJ, Zochodne DW (2012) Overexpression of human HSP27 protects sensory neurons from diabetes. Neurobiol Dis 47(3):436–443
36. Dixon WJ (1965) The up-and-down method for small samples. J Am Stat Assoc 60(312):967–978
37. Ward SJ, Ramirez MD, Neelakantan H, Walker EA (2011) Cannabidiol prevents the development of cold and mechanical allodynia in paclitaxel-treated female C57Bl6 mice. Anesth Analg 113(4):947–950
38. Choi Y, Yoon YW, Na HS, Kim SH, Chung JM (1994) Behavioral signs of ongoing pain and cold allodynia in a rat model of neuropathic pain. Pain 59(3):369–376
39. Materazzi S, Fusi C, Benemei S, Pedretti P, Patacchini R, Nilius B, Prenen J, Creminon C et al (2012) TRPA1 and TRPV4 mediate paclitaxel-induced peripheral neuropathy in mice via a glutathione-sensitive mechanism. Pflugers Arch 463(4):561–569
40. Decosterd I, Woolf CJ (2000) Spared nerve injury: an animal model of persistent peripheral neuropathic pain. Pain 87(2):149–158
41. Asthana P, Zhang N, Kumar G, Chine VB, Singh KK, Mak YL, Chan LL, Lam PKS et al (2018) Pacific ciguatoxin induces excitotoxicity and neurodegeneration in the motor cortex via caspase 3 activation: implication for irreversible motor deficit. Mol Neurobiol 55(8):6769–6787
42. Painter MW, Brosius Lutz A, Cheng YC, Latremoliere A, Duong K, Miller CM, Posada S, Cobos EJ et al (2014) Diminished Schwann cell repair responses underlie age-associated impaired axonal regeneration. Neuron 83(2):331–343
43. Bobylev I, Joshi AR, Barham M, Ritter C, Neiss WF, Höke A, Lehmann HC (2015) Paclitaxel inhibits mRNA transport in axons. Neurobiol Dis 82:321–331
44. Wozniak KM, Wu Y, Farah MH, Littlefield BA, Nomoto K, Slusher BS (2013) Neuropathy-inducing effects of eribulin mesylate versus paclitaxel in mice with preexisting neuropathy. Neurotox Res 24(3): 338–344
45. Ma KH, Hung HA, Srinivasan R, Xie H, Orkin SH, Svaren J (2015) Regulation of peripheral nerve myelin maintenance by gene repression through polycomb repressive complex 2. J Neurosci 35(22): 8640–8652
46. Boehmerle W, Huehnchen P, Peruzzaro S, Balkaya M, Endres M (2014) Electrophysiological, behavioral and histological characterization of paclitaxel, cisplatin, vincristine and bortezomib-induced neuropathy in C57Bl/6 mice. Sci Rep 4:6370
47. Cliffer KD, Siuciak JA, Carson SR, Radley HE, Park JS, Lewis DR, Zlotchenko E, Nguyen T et al (1998) Physiological characterization of Taxol-induced large-fiber sensory neuropathy in the rat. Ann Neurol 43(1):46–55
48. Huehnchen P, Boehmerle W, Endres M (2013) Assessment of paclitaxel induced sensory polyneuropathy with "Catwalk" automated gait analysis in mice. PLoS One 8(10):e76772
49. Quasthoff S, Hartung HP (2002) Chemotherapy-induced peripheral neuropathy. J Neurol 249(1):9–17
50. Sahenk Z, Barohn R, New P, Mendell JR (1994) Taxol neuropathy: electrodiagnostic and sural nerve biopsy findings. Arch Neurol 51(7):726–729
51. van den Bent MJ, van Raaij-van den Aarssen VJ, Verweij J, Doorn PA, Sillevis Smitt PA (1997) Progression of paclitaxel-induced neuropathy following discontinuation of treatment. Muscle Nerve 20(6):750–752
52. Flatters SJ, Bennett GJ (2006) Studies of peripheral sensory nerves in paclitaxel-induced painful peripheral neuropathy: evidence for mitochondrial dysfunction. Pain 122(3):245–257
53. Arrieta O, Hernandez-Pedro N, Fernández-González-Aragón M, Saavedra-Perez D, Campos-Parra A, Rios-Trejo M, Cerón-Lizárraga T, Martínez-Barrera L et al (2011) Retinoic acid reduces chemotherapy-induced neuropathy in an animal model and patients with lung cancer. Neurology 77(10):987–995
54. Lipton RB, Apfel SC, Dutcher JP, Rosenberg R, Kaplan J, Berger A, Einzig AI, Wiernik P et al (1989) Taxol produces a predominantly sensory neuropathy. Neurology 39(3):368–373
55. Chen X, Stubblefield MD, Custodio CM, Hudis CA, Seidman AD, DeAngelis LM (2013) Electrophysiological features of taxane-induced polyneuropathy in patients with breast cancer. J Clin Neurophysiol 30(2):199–203
56. Park SB, Lin CSY, Krishnan AV, Friedlander ML, Lewis CR, Kiernan MC (2011) Early, progressive, and sustained dysfunction of sensory axons underlies paclitaxel-induced neuropathy. Muscle Nerve 43(3):367–374
57. Weil MT, Mobius W, Winkler A, Ruhwedel T, Wrzos C, Romanelli E, Bennett JL, Enz L et al (2016) Loss of myelin basic protein function triggers myelin breakdown in models of demyelinating diseases. Cell Rep 16(2):314–322
58. Purves D, Augustine G, Fitzpatrick D, Katz L, LaMantia A, McNamara J, Williams S (2004) Increased conduction velocity as a result of myelination. Neuroscience. In: Neuroscience, 3nd edn. Sinauer Associates, Sunderland, pp 63–65
59. Flatters SJ, Xiao W-H, Bennett GJ (2006) Acetyl-L-carnitine prevents and reduces paclitaxel-induced painful peripheral neuropathy. Neurosci Lett 397(3):219–223
60. Xiao WH, Bennett GJ (2012) Effects of mitochondrial poisons on the neuropathic pain produced by the chemotherapeutic agents, paclitaxel and oxaliplatin. Pain 153(3):704–709
61. Griffiths LA, Flatters SJ (2015) Pharmacological modulation of the mitochondrial electron transport chain in paclitaxel-induced painful peripheral neuropathy. J Pain 16(10):981–994
62. Krukowski K, Nijboer CH, Huo X, Kavelaars A, Heijnen CJ (2015) Prevention of chemotherapy-induced peripheral neuropathy by the small-molecule inhibitor pifithrin-μ. Pain 156(11):2184–2192
63. Joseph EK, Levine JD (2006) Mitochondrial electron transport in models of neuropathic and inflammatory pain. Pain 121(1):105–114
64. Zheng H, Xiao WH, Bennett GJ (2012) Mitotoxicity and bortezomib-induced chronic painful peripheral neuropathy. Exp Neurol 238(2):225–234
65. Neumar RW, Xu YA, Gada H, Guttmann RP, Siman R (2003) Cross-talk between calpain and caspase proteolytic systems during neuronal apoptosis. J Biol Chem 278(16):14162–14167
66. Huang ZZ, Li D, Liu CC, Cui Y, Zhu HQ, Zhang WW, Li YY, Xin WJ (2014) CX3CL1-mediated macrophage activation contributed to paclitaxel-induced DRG neuronal apoptosis and painful peripheral neuropathy. Brain Behav Immun 40:155–165
67. Friesland A, Weng Z, Duenas M, Massa SM, Longo FM, Lu Q (2014) Amelioration of cisplatin-induced experimental peripheral

neuropathy by a small molecule targeting p75 NTR. Neurotoxicology 45:81–90
68. James SE, Burden H, Burgess R, Xie Y, Yang T, Massa SM, Longo FM, Lu Q (2008) Anti-cancer drug induced neurotoxicity and identification of Rho pathway signaling modulators as potential neuroprotectants. Neurotoxicology 29(4):605–612
69. James SE, Dunham M, Carrion-Jones M, Murashov A, Lu Q (2010) Rho kinase inhibitor Y-27632 facilitates recovery from experimental peripheral neuropathy induced by anti-cancer drug cisplatin. Neurotoxicology 31(2):188–194
70. Qiu Y, Chen WY, Wang ZY, Liu F, Wei M, Ma C, Huang YG (2016) Simvastatin attenuates neuropathic pain by inhibiting the RhoA/LIMK/cofilin pathway. Neurochem Res 41(9):2457–2469
71. Scuteri A, Nicolini G, Miloso M, Bossi M, Cavaletti G, Windebank AJ, Tredici G (2006) Paclitaxel toxicity in post-mitotic dorsal root ganglion (DRG) cells. Anticancer Res 26(2A):1065–1070
72. Melli G, Taiana M, Camozzi F, Triolo D, Podini P, Quattrini A, Taroni F, Lauria G (2008) Alpha-lipoic acid prevents mitochondrial damage and neurotoxicity in experimental chemotherapy neuropathy. Exp Neurol 214(2):276–284
73. Liu XJ, Zhang Y, Liu T, Xu ZZ, Park CK, Berta T, Jiang D, Ji RR (2014) Nociceptive neurons regulate innate and adaptive immunity and neuropathic pain through MyD88 adapter. Cell Res 24(11): 1374–1377
74. Berta T, Park CK, Xu ZZ, Xie RG, Liu T, Lu N, Liu YC, Ji RR (2014) Extracellular caspase-6 drives murine inflammatory pain via microglial TNF-alpha secretion. J Clin Invest 124(3):1173–1186
75. Berta T, Qadri YJ, Chen G, Ji RR (2016) Microglial signaling in chronic pain with a special focus on caspase 6, p38 MAP kinase, and sex dependence. J Dent Res 95(10):1124–1131
76. Benn SC, Perrelet D, Kato AC, Scholz J, Decosterd I, Mannion RJ, Bakowska JC, Woolf CJ (2002) Hsp27 upregulation and phosphorylation is required for injured sensory and motor neuron survival. Neuron 36(1):45–56
77. André N, Braguer D, Brasseur G, Gonçalves A, Lemesle-Meunier D, Guise S, Jordan MA, Briand C (2000) Paclitaxel induces release of cytochrome c from mitochondria isolated from human neuroblastoma cells. Cancer Res 60(19):5349–5353
78. Mehlen P, Kretz-Remy C, Preville X, Arrigo A-P (1996) Human hsp27, Drosophila hsp27 and human alphaB-crystallin expression-mediated increase in glutathione is essential for the protective activity of these proteins against TNFalpha-induced cell death. EMBO J 15(11):2695–2706
79. Wang C, Song S, Zhang Y, Ge Y, Fang X, Huang T, Du J, Gao J (2015) Inhibition of the Rho/Rho kinase pathway prevents lipopolysaccharide-induced hyperalgesia and the release of TNF-alpha and IL-1beta in the mouse spinal cord. Sci Rep 5:14553
80. Zulauf L, Coste O, Marian C, Moser C, Brenneis C, Niederberger E (2009) Cofilin phosphorylation is involved in nitric oxide/cGMP-mediated nociception. Biochem Biophys Res Commun 390(4): 1408–1413
81. Wu KY, Hengst U, Cox LJ, Macosko EZ, Jeromin A, Urquhart ER, Jaffrey SR (2005) Local translation of RhoA regulates growth cone collapse. Nature 436(7053):1020–1024
82. Qin Q, Baudry M, Liao G, Noniyev A, Galeano J, Bi X (2009) A novel function for p53: regulation of growth cone motility through interaction with Rho kinase. J Neurosci 29(16):5183–5192
83. Tanaka H, Yamashita T, Asada M, Mizutani S, Yoshikawa H, Tohyama M (2002) Cytoplasmic p21(Cip1/WAF1) regulates neurite remodeling by inhibiting Rho-kinase activity. J Cell Biol 158(2):321–329
84. Sun X, Zhou Z, Fink DJ, Mata M (2013) HspB1 silences translation of PDZ-RhoGEF by enhancing miR-20a and miR-128 expression to promote neurite extension. Mol Cell Neurosci 57:111–119
85. Chandran V, Coppola G, Nawabi H, Omura T, Versano R, Huebner EA, Zhang A, Costigan M et al (2016) A systems-level analysis of the peripheral nerve intrinsic axonal growth program. Neuron 89(5):956–970